

This discussion paper is/has been under review for the journal Hydrology and Earth System Sciences (HESS). Please refer to the corresponding final paper in HESS if available.

# Inter-comparison of energy balance and hydrological models for land surface energy fluxes estimation over a whole river catchment

R. Guzinski<sup>1</sup>, H. Nieto<sup>1</sup>, S. Stisen<sup>2</sup>, and R. Fensholt<sup>1</sup>

<sup>1</sup>Department of Geosciences and Natural Resource Management, University of Copenhagen, Øster Voldgade 10, 1350 Copenhagen, Denmark

<sup>2</sup>Geological Survey of Denmark and Greenland, Øster Voldgade 10, 1350 Copenhagen, Denmark

Received: 23 April 2014 – Accepted: 13 May 2014 – Published: 6 June 2014

Correspondence to: R. Guzinski (rag@ign.ku.dk, rmgu@dhi-gras.com)

Published by Copernicus Publications on behalf of the European Geosciences Union.

HESSD

11, 5905–5951, 2014

Inter-comparison of  
energy balance and  
hydrological models  
over a whole river  
catchment

R. Guzinski et al.

<a href="#">Title Page</a>	
<a href="#">Abstract</a>	<a href="#">Introduction</a>
<a href="#">Conclusions</a>	<a href="#">References</a>
<a href="#">Tables</a>	<a href="#">Figures</a>
<a href="#"></a>	<a href="#"></a>
<a href="#"></a>	<a href="#"></a>
<a href="#">Back</a>	<a href="#">Close</a>
<a href="#">Full Screen / Esc</a>	

<a href="#">Printer-friendly Version</a>
<a href="#">Interactive Discussion</a>

## Abstract

Evapotranspiration is the main link between the natural water cycle and the land surface energy budget. Therefore water-balance and energy-balance approaches are two of the main methodologies for modelling of this process. The water-balance approach ensures that the amount of water coming into a system, mainly through precipitation, is balanced by the amount of water leaving the system through evapotranspiration, runoff and other processes. This modelling methodology is usually implemented as a complex, distributed hydrological model. The energy-balance approach ensures the conservation of energy at the land surface and is often used with remotely sensed observations of, for example, the land surface temperature (LST) and the state of the vegetation. In this study we compare the catchment scale output of two remote sensing models based on the Two-Source Energy Balance (TSEB) scheme, against a hydrological model, MIKE SHE, calibrated over the Skjern river catchment in western Denmark, the area covered by the Danish Hydrological Observatory (HOBE). The first TSEB model utilizes the time differential LST measurements provided by the night and day overpasses of the MODIS sensor aboard the Aqua satellite, while the second uses the dual-angle LST measurements made available by the AATSR sensor that used to fly on the Envisat satellite. All three models use the same ancillary data (meteorological measurements, land cover type and leaf area index, etc.) and produce output at similar spatial resolution (1 km for the TSEB models, 500 m for MIKE SHE). The comparison is performed on the spatial patterns of the fluxes present within the catchment area as well as on temporal patterns visible in 7 year long time series. The results aid the understanding of strengths and weaknesses of each modelling approach and explore the benefits to the hydrological modelling community of evapotranspiration maps derived with the energy-balance methodology.

## Inter-comparison of energy balance and hydrological models over a whole river catchment

R. Guzinski et al.

[Title Page](#)

[Abstract](#)

[Introduction](#)

[Conclusions](#)

[References](#)

[Tables](#)

[Figures](#)

◀

▶

◀

▶

[Back](#)

[Close](#)

[Full Screen / Esc](#)

[Printer-friendly Version](#)

[Interactive Discussion](#)

# 1 Introduction

Evapotranspiration (ET) acts as a coupling between two of the most important natural processes affecting the land surface: the water (mass) exchange and energy exchange (Campbell and Norman, 1998). Therefore it has a strong impact on, and is impacted by, 5 plant biophysics, weather and climate and is an important component when modelling those processes. At the same time the knowledge of the magnitude of water loss from the ground through evapotranspiration, as well as spatial distribution of this flux, has many practical applications, such as in agri- and aquaculture, water resource management or drought monitoring (Anderson et al., 2012). This has led to an 10 active interest from the research community in the spatially distributed modelling of evapotranspiration and to the development of a number of different methodologies. Two of the most common approaches are: (1) the modelling of land-surface energy fluxes, mostly with the use of land surface temperature (LST) maps derived from remote sensing observations; and (2) distributed physically-based hydrological models.

15 The two types of modelling approaches have been compared previously, for example recently by Conradt et al. (2013) who compared ET patterns produced by hydrological model, remote sensing based model and ground measurements in sub-basins of the Elbe river. That paper concluded with a recommendation of further comparison studies 20 of the different modelling approaches, especially using more than two independent models, to better understand their relative strengths and weaknesses. This should lead to improved model performance but also to increased understanding of the errors (and their magnitudes) present in the different models, which is particularly important if the approaches are to be combined through, for example, data assimilation. Without the knowledge of errors, assimilating remotely sensed ET into hydrological 25 models might not provide its full benefit. Pan et al. (2008), for example, found that assimilating ET derived with remote sensing observations into their hydrological model did not have a large impact on the modelled water budget since it was assumed that the calibrated hydrological model provided much more accurate ET values than

## Inter-comparison of energy balance and hydrological models over a whole river catchment

R. Guzinski et al.

[Title Page](#)

[Abstract](#)

[Introduction](#)

[Conclusions](#)

[References](#)

[Tables](#)

[Figures](#)

[◀](#)

[▶](#)

[◀](#)

[▶](#)

[Back](#)

[Close](#)

[Full Screen / Esc](#)

[Printer-friendly Version](#)

[Interactive Discussion](#)

the satellite observation based model. Schuurmans et al. (2011) found that although spatial patterns produced by the hydrological model became more realistic after the assimilation of satellite based ET, a major weakness was the lack of information about the standard error present in the ET estimates and lack of independent spatially distributed ET dataset that could be used for validation. Therefore, in this study we compare two remote sensing based ET models and a hydrological model, with the aim of improving the understanding of their limitations and providing information that could be used in potential future integration of the approaches through data assimilation.

The remote sensing models of evapotranspiration (Kalma et al., 2008) aspire to minimize the calibration of site specific parameters and the usage to locally derived data. Instead they aim to be applicable in a wide number of climatic and vegetation conditions without any major modifications, and to rely mostly on data acquired through satellite observations (e.g. LST) or regional scale modelling (e.g. air temperature). This necessitates in a number of assumptions and simplifications, which might lead to reduced accuracy of the modelled fluxes. Another feature of the remote sensing models is the treatment of each pixel within the modelling domain as a stand-alone sub-domain without any connections or interactions with the surrounding pixels. In some approaches, such as the triangle approach (see below), some of the model parameters are derived through common analysis of all the pixels in the domain but the fluxes in the individual pixels are still derived individually. Similarly, the remote sensing models consider each satellite image as a stand-alone snapshot of the land surface conditions with no memory of the past.

There are a number of remote sensing modelling methodologies being actively used by the research community ranging from simpler, empirical ones to more complex, physically based ones. One of the simpler approaches consist of the so-called “triangle” models, named after the shape resulting from plotting the pixel values of an LST map against pixel values of a vegetation index map. The evaporation fraction can then be derived by interpolating between the edges of the triangle (Jiang and Islam, 2001; Stisen et al., 2008). More advanced schemes characterize the ground surface as

one layer (soil and vegetation combined) in one-source models (e.g. Surface Energy Balance System model, Su, 2002), or as two layers (soil and vegetation separately) in two-source models, majority of which follow the Two Source Energy Balance (TSEB) modelling scheme (Norman et al., 1995). Both the one-source and two-source models

5 characterize the fluxes of heat and moisture between the surface and the atmosphere in terms of a set of resistance equations, formulated from physically based models of boundary layer behaviour under different atmospheric conditions and vegetation covers. The two-source models have the advantage of being more physically realistic and avoiding certain parametrization issues present in the one-source models (Norman et al., 1995).

10 The distributed physically-based hydrological models, in contrast to the remote sensing models, are heavily parametrized and calibrated for each individual catchment or study area (Refsgaard, 1997). Besides evapotranspiration, and other land surface fluxes, they can model a host of other hydrological processes such as channel flow, 15 unsaturated zone flow or ground water flow and the interactions between those processes (Graham and Butts, 2005). This means that the modelling is performed in 4 dimensions (latitude, longitude, elevation or depth, and time) and that there is an interaction between the model pixels in both time and space. Due to their complex nature the hydrological models require significant computational resources 20 and large number of inputs for calibration and operation. During the operational stage the models require gridded meteorological input (including rainfall, air temperature and humidity), gridded soil hydraulic parameters and digital elevation model among others (Stisen et al., 2011a). During the calibration stage (prior to the operational stage) additional information is required, for example measured hydrological parameters such 25 as hydraulic head or stream outflow.

Since the hydrological models are calibrated using detailed hydrological observations it is our hypothesis that the catchment wide evapotranspiration estimated by those models is more accurate than the one derived with remote sensing models. On the other hand, we expect the energy balance models driven by remote sensing

observations to better represent the spatial patterns of the fluxes present within the catchment. We evaluate this hypothesis by running a hydrological model, MIKE SHE, described in Sect. 4.1, and two TSEB based models, Dual-Temperature-Difference (DTD – Norman et al., 2000; Guzinski et al., 2013) and TSEB-2 Angle Radiative Transfer (TSEB-2ART – Nieto et al., 2013), described in Sect. 4.2, over the Skjern river catchment located in western Denmark (see Sect. 2). Apart from being the largest river in Denmark, Skjern is also the study area of the Danish hydrological observatory HOBE (Jensen and Illangasekare, 2011), thus providing ample data for calibrating and validating the models. The three models are run with the same meteorological inputs, interpolated from field based observations, and the same land cover and leaf area index (LAI) maps, in order to minimize the uncertainties inherent from using different datasets. The differences between the models, and their input data, are described in Sect. 4.

The output land surface fluxes, and in particular the latent heat flux, from the three models are then inter-compared. The comparison is performed on pixel-by-pixel basis as well as on catchment scale and both systematic and unsystematic differences are analysed (Ji and Gallo, 2006). In addition, the catchment-scale temporal evolution of the evapotranspiration estimated from the three models is evaluated. Through this, we assess strengths and weaknesses of the different modelling approaches and in particular discuss the benefits to the hydrological modeller of obtaining some of the model inputs through remotely sensed energy balance approach.

## 2 Study area

The study area covers the Skjern river catchment (Fig. 1) which is located on the western part of Denmark's Jutland peninsula and it is the largest river catchment in Denmark in terms of water volume. It has a roughly rectangular shape with the east-west length of around 60 km and north-south length of around 40 km. The Skjern river outlet is on the western side of the catchment with the discharge entering the

<a href="#">Title Page</a>	
<a href="#">Abstract</a>	<a href="#">Introduction</a>
<a href="#">Conclusions</a>	<a href="#">References</a>
<a href="#">Tables</a>	<a href="#">Figures</a>
<a href="#">◀</a>	<a href="#">▶</a>
<a href="#">◀</a>	<a href="#">▶</a>
<a href="#">Back</a>	<a href="#">Close</a>
<a href="#">Full Screen / Esc</a>	
<a href="#">Printer-friendly Version</a>	
<a href="#">Interactive Discussion</a>	

Ringkøbing Fjord. The terrain is mostly flat with a maximum elevation of 125 m a.s.l. and a gentle east to west slope. The soils are predominantly sandy with the main land use being agriculture and coniferous plantations. The catchment experiences temperate maritime climate, with mean annual precipitation of 990 mm and mean annual temperature of 8.2 °C. Since 2007 the catchment is hosting the Danish Hydrological Observatory, HOBE, with numerous experiments and measurements concerning precipitation, evapotranspiration, greenhouse gas exchange, ground-surface water interactions and other related topics, making it highly suitable for calibrating and evaluating the distributed physically-based hydrological models. For more details refer to Jensen and Illangasekare (2011).

### 3 Common model inputs

In order to compare the performance of the three models and not the accuracy of their inputs, the models used the same auxiliary input data whenever possible. Those common inputs consisted of maps with meteorological forcings, LAI, albedo and land cover types. For the meteorological forcing data, kriged fields of wind and temperature corrected precipitation from 43 rain gauges were used (Stisen et al., 2011b) together with air temperature, relative humidity, incoming shortwave radiation, wind speed and pressure interpolated from 16 climate stations. The locations of the rain gauges and climate stations in relation to the study area are presented in Fig. 2 of Stisen et al. (2011a). The vegetation related inputs were derived using remote sensing data with LAI estimated from MODIS NDVI (MOD13A1 product) following the study of Boegh et al. (2009) and albedo estimated from narrow band MODIS reflectance following Liang (2001). It should be noted that albedo maps were only shared by MIKE SHE and DTD with TSEB-2ART producing its own albedo maps as one of the outputs. Land cover map was taken from the Danish Areal Information System run by the Danish Ministry of Environment ([http://www2.dmu.dk/1\\_Viden/2\\_Miljoe-tilstand/3\\_samfund/AIS/1a\\_](http://www2.dmu.dk/1_Viden/2_Miljoe-tilstand/3_samfund/AIS/1a_)

<a href="#">Title Page</a>	
<a href="#">Abstract</a>	<a href="#">Introduction</a>
<a href="#">Conclusions</a>	<a href="#">References</a>
<a href="#">Tables</a>	<a href="#">Figures</a>
<a href="#">◀</a>	<a href="#">▶</a>
<a href="#">◀</a>	<a href="#">▶</a>
<a href="#">Back</a>	<a href="#">Close</a>
<a href="#">Full Screen / Esc</a>	
<a href="#">Printer-friendly Version</a>	
<a href="#">Interactive Discussion</a>	

The LST observations used by the different models, as well as data used only by a single model, are described in the sections below.

## 5 4 Models

### 4.1 MIKE-SHE model

The implementation details of the hydrological model used in this study, MIKE SHE SW-ET, are presented in Stisen et al. (2011a) and Overgaard and Rosbjerg (2005). Briefly, the model couples ground-water and surface-water modules together with an ET module (Overgaard and Rosbjerg, 2005). The SW-ET module, based on the two source model of Shuttleworth and Wallace (1985), uses hydrological modules' outputs of soil moisture, soil heat flux and fraction of soil and leaf covered by ponded water. Besides of these parameters, meteorological observations of air temperature and humidity, wind speed and incoming shortwave radiation and maps of albedo, LAI and landcover are used to solve a set of 10 linear equations for the temperature and humidity of dry and wet soil, dry and wet leaf and inter-canopy air (see Appendices A and D in Overgaard and Rosbjerg, 2005, for more details). With those parameters it is possible to estimate the effective soil and leaf temperatures as well as the radiometric surface temperature (LST) and the latent and sensible heat fluxes. Since the model simulates LST, it is possible to calibrate the model against remotely sensed LST in addition to hydrological variables such as hydraulic head or stream outflow. The model used in this study was calibrated for the Skjern river catchment against the above mentioned hydrological variables, LST taken from the MYD11A1 Aqua-MODIS product, evapotranspiration measured at three flux tower sites placed within the catchment area and soil moisture measurements from a distributed sensor network. The calibration methodology will be a topic of a subsequent paper.

As input the model requires gridded meteorological forcing data, soil hydraulic parameters and a number of parameters related to vegetation. The meteorological forcing data, LAI, albedo and land use maps are described in Sect. 3. The soil hydraulic parameters came from a study of Greve et al. (2007). The derivation of other input parameters, such as soil surface roughness or irrigation water input, is described in Stisen et al. (2011a). The MIKE SHE SW-ET model, from now on referred to as MIKE SHE, was run at 500 m resolution and as output provided the surface energy fluxes (sensible, latent and ground heat fluxes and net radiation) together with LST and soil and canopy temperatures,  $T_S$  and  $T_C$  respectively. The outputs were bilinearly interpolated from 500 m to 1 km to match the resolution of the outputs from both remote sensing models.

## 4.2 TSEB modelling scheme

The TSEB approach (Norman et al., 1995) splits the observed LST into its two main components, namely the temperature of soil and canopy:

$$T_R(\theta) \approx \left[ f(\theta)T_C^4 + (1 - f(\theta))T_S^4 \right]^{0.25} \quad (1)$$

where  $T_R(\theta)$  is the LST observed at view zenith angle (VZA) of  $\theta$  and  $f(\theta)$  is the fraction of vegetation cover in the field of view of the sensor at VZA  $\theta$ . This allows the model to estimate the latent and sensible heat fluxes from the soil and canopy separately thus avoiding the need to parametrize “excess” resistance term which is often present in single-source models (Norman et al., 1995).

In the single-angle TSEB models, the latent heat flux of the canopy,  $LE_C$ , is initially estimated using the assumption that the canopy is transpiring at the potential rate dictated by the divergence of net radiation in the canopy,  $R_{n,C}$ , and a modified Priestly–Taylor approach. This allows an initial estimation of the sensible heat flux of the canopy,  $H_C$ , and of  $T_C$ . If the model returns unrealistic results ( $LE < 0$  meaning condensation

<a href="#">Title Page</a>	
<a href="#">Abstract</a>	<a href="#">Introduction</a>
<a href="#">Conclusions</a>	<a href="#">References</a>
<a href="#">Tables</a>	<a href="#">Figures</a>
<a href="#">◀</a>	<a href="#">▶</a>
<a href="#">◀</a>	<a href="#">▶</a>
<a href="#">Back</a>	<a href="#">Close</a>
<a href="#">Full Screen / Esc</a>	
<a href="#">Printer-friendly Version</a>	
<a href="#">Interactive Discussion</a>	

during daytime) the transpiration of the canopy can be iteratively reduced until realistic results are obtained (Norman et al., 1995).

In the dual-angle TSEB models,  $T_S$  and  $T_C$  can be derived directly from the observation geometry, followed by  $H_S$  and  $H_C$  and finally  $LE_C$  as residual of the canopy energy balance. In both cases the total energy balance is ensured by estimating the latent heat flux from the soil,  $LE_S$ , as residual:

$$\text{LE}_S = R_{n,S} - H_S - G = (R_n - R_{n,C}) - (H - H_C) - G \quad (2)$$

where  $R_{n,S}$  is the net radiation of the soil,  $H_S$  is the sensible heat flux of the soil and  $G$  is the ground heat flux.

The two TSEB based models used in this study follow the principles described above but differ in other implementation details as described in the subsections below.

#### 4.2.1 DTD model

The DTD model minimizes the influence of systematic error in the retrievals of LST and air temperature by replacing absolute temperature measurements with temperature change between two observations (Norman et al., 2000). In the original DTD model the first observations was early in the morning, when fluxes are minimal, and the second later in the morning or in the afternoon. Guzinski et al. (2013) demonstrated that replacing the early morning observations with night time ones does not have a significant effect on the modelled fluxes, therefore facilitating the use of polar orbiting satellites with day and night overpasses, and introduced a simple scheme for accounting for vegetation phenology when estimating canopy transpiration. The model was further modified in Guzinski et al. (2014) where the resistance network to sensible heat flux was modified, to the so-called “series” configuration, to explicitly consider the in-canopy air temperature, thus improving the model performance during dry conditions. The DTD model formulation used in this study is as described in the appendices of Guzinski et al. (2014), with the exception of the formulation of the resistance to heat transfer from the soil surface,  $R_S$ .

## Inter-comparison of energy balance and hydrological models over a whole river catchment

R. Guzinski et al.

## Title Page

## Abstract

## Introduction

## Conclusions

## References

## Tables

## Figures

1

1

5

1

Back

Close

Full Screen / Esc

[Printer-friendly Version](#)

## Interactive Discussion



$R_S$  formulation used in the TSEB modelling scheme accounts for turbulent transport from free convection (Kustas and Norman, 1999):

$$R_S = \frac{1}{c(T_S - T_C)^{1/3} + bu_S} \quad (3)$$

5 where  $c$  and  $b$  are constants given a value of  $0.0025 \text{ m s}^{-1} \text{ K}^{-1/3}$  and  $0.012 \text{ m s}^{-1}$  respectively and  $u_S$  is the wind speed just above the soil surface. However, in DTD this formulation was modified to avoid the use of absolute temperature estimations and the  $c(T_S - T_C)^{1/3}$  term was given a constant value of 0.004 for LAI larger than 2 and 0.006 for LAI smaller than 2 (Norman et al., 2000), thus assuming  $T_S$  to  $T_C$  difference for dense canopies of around 5 K and 15 K in case of sparse canopies. Those 10 assumptions made sense for the data sets used to evaluate the model performance, taken in New Mexico over June and July 1997 (<http://hydrolab.arsusda.gov/sgp97>, last accessed 27 February 2014) and in Arizona from June to September 1990 (Kustas and Goodrich, 1994). However, in the current study area, dominated by croplands 15 located in temperate maritime climate (see Sect. 2), sparse canopy conditions are usually present in early spring and autumn when the difference between  $T_S$  to  $T_C$  is significantly less than 15 K. Therefore the  $R_S$  formulation was further modified to make use of the difference in thermal inertia of LST and air temperature:

$$R_S = \frac{1}{c[(T_{R,1} - T_{R,0}) - (T_{A,1} - T_{A,0})]^{1/3} + bu_S} \quad (4)$$

20 where subscript 0 indicates temperatures estimate at night or early in the morning, and 1 indicates estimate at some other time during the day, and  $b$  and  $c$  have the same values as shown above. This formulation implicitly takes into account the amount of 25 vegetation cover, since vegetation has larger thermal inertia than soil and thus  $(T_{R,1} - T_{R,0})$  is lower for dense canopies, while also reflecting the climatic conditions present in the study area.

<a href="#">Title Page</a>	
<a href="#">Abstract</a>	<a href="#">Introduction</a>
<a href="#">Conclusions</a>	<a href="#">References</a>
<a href="#">Tables</a>	<a href="#">Figures</a>
<a href="#">◀</a>	<a href="#">▶</a>
<a href="#">◀</a>	<a href="#">▶</a>
<a href="#">Back</a>	<a href="#">Close</a>
<a href="#">Full Screen / Esc</a>	
<a href="#">Printer-friendly Version</a>	
<a href="#">Interactive Discussion</a>	

The model uses MODIS LST estimates from the MYD11A1 product, together with land cover, LAI and albedo values derived as described in Sect. 3 and vegetation indices (Normalised Difference Vegetation Index and Enhanced Vegetation Index) from the MOD13A2 product for estimating the fraction of vegetation that is green (Guzinski et al., 2013). The meteorological inputs are also as described in Sect. 3. The modelled fluxes are output at 1 km resolution.

#### 4.2.2 TSEB-2ART model

The TSEB-2ART model (Nieto et al., 2013) couples a dual angle version of TSEB introduced by Kustas and Norman (1997), with a radiative transfer model (RTM) 4SAIL (Verhoef et al., 2007). Through this coupling it is possible to retrieve canopy and soil temperatures by inverting the RTM with LST estimates of the same area but obtained through two different view zenith angles. 4SAIL takes into account the different emissivities of the end members (canopy and soil) and hence multiple scattering of the thermal radiation, as well as the downwelling longwave radiation reflected by the surface. Therefore, the coupling should result in more accurate temperature retrievals compared to just using the geometric configuration of the observations (Nieto et al., 2013). In addition the RTM is used to estimate the net radiation, and radiation divergence in the canopy, while taking into account multiple scattering of the short/long wave radiation between the soil and the canopy and within the canopy. Finally, the inclusion of 4SAIL allows for the use of different leaf inclination distribution functions, rather than the spherical leaf distribution of the original TSEB (Norman et al., 1995; Kustas and Norman, 1999).

TSEB-2ART has been evaluated over three flux tower sites within the HOBE area, obtaining more accurate flux retrievals than both the original dual angle (Kustas and Norman, 1997) and the single angle TSEB (Norman et al., 1995) implementations when driven by LST estimates derived with the AATSR sensor on board the Envisat satellite (Nieto et al., 2013). Even though the Envisat satellite is no longer functional the model can be applied to the dual angle LST observations in the future Sentinel

[Title Page](#)

[Abstract](#)

[Introduction](#)

[Conclusions](#)

[References](#)

[Tables](#)

[Figures](#)

[◀](#)

[▶](#)

[◀](#)

[▶](#)

[Back](#)

[Close](#)

[Full Screen / Esc](#)

[Printer-friendly Version](#)

[Interactive Discussion](#)

3 mission (Donlon et al., 2012). Apart from the Envisat derived LST the model uses the same meteorological data and land cover and LAI maps as MIKE SHE and DTD models and produces albedo as one of the outputs. The fluxes are output at 1 km resolution.

## 5 Comparison methodology

The spatial comparison was performed by selecting all the pixels in the Skjern catchment on all the days between 2003 and 2010 when at least 10 % of the catchment was cloud free during the night and day Aqua overpasses and which met the following conditions:

- 10 – the pixel is not classified as water or urban area;
- all three models produce valid results, meaning  $LE > 0 \text{ W m}^{-2}$  and  $H \geq -100 \text{ W m}^{-2}$ ;
- the aerodynamic resistance of TSEB-2ART model has a realistic value, as in some model runs it was observed that TSEB-2ART modelled extremely high unstable conditions which lead to very low aerodynamic values.

15 This resulted in over 105 000 pixel sets to be compared. A median moving-window filter of  $3 \times 3$  pixels was applied to the output maps to reduce noise caused by image misregistration while preserving the spatial patterns found in the maps.

20 The comparison was performed using the modelled sensible heat flux, latent heat flux and Available Energy (AE) defined as net radiation minus the ground heat flux. The magnitude of those fluxes is strongly influenced by the incoming solar radiation and so it has a cyclic annual component with generally larger fluxes during the summer months and lower during the winter months. This could potentially influence the correlation between the fluxes modelled with different models. To remove this time dependent component and instead to evaluate the influence of water availability on the partitioning

of the available energy into latent and sensible heat fluxes by the different models, the Evaporative Fraction (EF), defined as the ratio of energy used for evapotranspiration to total available energy, was also used during the comparison.

When comparing the fluxes estimated by the three different models the hour at which the fluxes are estimated must be taken into account. The TSEB-2ART fluxes are estimated at the time of the Envisat overpass, which is around 11:30 Local Time (LT), while the DTD fluxes are estimated at the time of Aqua overpass, around 12:00–13:00 LT. The MIKE SHE fluxes are estimated at hourly intervals throughout the day. Therefore, when comparing the fluxes between MIKE SHE and one of the satellite based models a linear interpolation was performed between the two MIKE SHE estimates bracketing the satellite based estimate. When comparing the fluxes from two satellite based models there is an offset present due to this time difference, although it should be reduced when comparing EF (Peng et al., 2013).

A number of statistical measures are used to explore the relation between the fluxes, and temperatures, estimated by the three models. The first one is the Pearson correlation coefficient,  $r$ , which measures the linear covariation of two datasets. To assess the differences between the datasets the Root Mean Square Difference (RMSD), which is the square root of the Mean Square Difference (MSD), is used:

$$\text{RMSD} = \text{MSD}^{0.5} = \left[ \frac{1}{n} \sum_{i=1}^n (X_i - Y_i)^2 \right]^{0.5} \quad (5)$$

where  $X_i$  and  $Y_i$  are the  $i$ th points in the  $X$  and  $Y$  datasets. The MSD can be further split into systematic and unsystematic Mean Product-Differences (MPD),  $\text{MPD}_s$  and  $\text{MPD}_u$  respectively, where  $\text{MPD}_s$  measures the distance between the geometric mean regression line (Barker et al., 1988) of two datasets and the 1–1 line while  $\text{MPD}_u$  measures the distance between the datasets' points and the geometric mean regression line (Ji and Gallo, 2006). The geometric mean regression is used instead of the linear regression since the former one assumes that both  $X$  and  $Y$  are subject to errors. Since  $\text{MSD} = \text{MPD}_s + \text{MPD}_u$  it is also possible to calculate the relative

## Inter-comparison of energy balance and hydrological models over a whole river catchment

R. Guzinski et al.

[Title Page](#)

[Abstract](#)

[Introduction](#)

[Conclusions](#)

[References](#)

[Tables](#)

[Figures](#)

[◀](#)

[▶](#)

[◀](#)

[▶](#)

[Back](#)

[Close](#)

[Full Screen / Esc](#)

[Printer-friendly Version](#)

[Interactive Discussion](#)

contribution of the systematic and unsystematic difference to the total difference as  $MPD_s/MSD$  and  $MPD_u/MSD$  respectively (Ji and Gallo, 2006). The systematic component of the difference represents the variation between the datasets that can be corrected by simple linear transformation of one of the datasets, while the unsystematic difference can be thought of as noise caused by some unknown factors which is harder to correct for (Ji et al., 2008). For presentation purposes a square root is taken of  $MPD_s$  and  $MPD_u$  to obtain  $RMPD_s$  and  $RMPD_u$  respectively which are then shown in the results' tables. The last statistical measure used is the mean bias, calculated as the difference between the means of two datasets. With the exception of the sign of the bias all the statistical measures are symmetric, meaning that no assumption is made on the correctness or otherwise of any of the datasets and that the same values are obtained if the order of the datasets is reversed when calculating the measures.

The temporal patterns of evapotranspiration were evaluated at catchment scale, meaning that all the valid non-urban and non-water pixels within the catchment were averaged to determine the catchment scale fluxes. It should be noted that since MIKE SHE also simulates the fluxes over water and urban pixels, this average is not the whole catchment evapotranspiration as modelled by MIKE SHE. However, since the number of water and urban pixels is quite small (Fig. 1) the averaged value should be close to the whole catchment evapotranspiration. Only those days on which the remote sensing models produced flux estimates in pixels representing at least 80 % of all non-urban and non-water catchment pixels were included in the analysis. In case of DTD this condition was satisfied on 92 days over the 7 year period, while in case of TSEB-2ART there were 72 valid days due to the less frequent revisit time of AATSR vs. MODIS. The catchment averages for each date were produced using the same set of pixels for the remote sensing models and MIKE SHE. The two datasets were compared using the  $r$  correlation coefficient, RMSD and bias and the ratio of RMSD and bias to the mean evapotranspiration estimated by MIKE SHE.

## Inter-comparison of energy balance and hydrological models over a whole river catchment

R. Guzinski et al.

[Title Page](#)

[Abstract](#)

[Introduction](#)

[Conclusions](#)

[References](#)

[Tables](#)

[Figures](#)

[◀](#)

[▶](#)

[◀](#)

[▶](#)

[Back](#)

[Close](#)

[Full Screen / Esc](#)

[Printer-friendly Version](#)

[Interactive Discussion](#)

## 6 Results

### 6.1 Spatial patterns

The results of pixel-to-pixel comparisons of fluxes between the three model pairs are presented in Figs. 2 (MIKE SHE–DTD), 3 (MIKE SHE–TSEB-2ART), and 4 (TSEB-  
5 2ART–DTD) with statistics summarized in Table 2 and described for each model pair in the subsections below.

#### 6.1.1 MIKE SHE vs. DTD

The bias between the turbulent fluxes modelled with MIKE SHE and DTD is small with a value of  $-4 \text{ W m}^{-2}$  and  $-9 \text{ W m}^{-2}$  for  $H$  and  $LE$  respectively. However, the  
10 RMSD is significant, at  $78 \text{ W m}^{-2}$  for  $H$  and  $97 \text{ W m}^{-2}$  for  $LE$ , and consequently the correlation coefficient between the modelled turbulent fluxes is relatively low, with a maximum value of 0.54. This is also reflected in the split of the differences between systematic and unsystematic parts, with over 95 % of the difference for both the fluxes being unsystematic. The differences are propagated through to EF, leading to very  
15 low correlation although with a negligible bias. The differences in the turbulent fluxes cannot be caused by differences in the parametrization of the available energy since in that case the correlation reaches 0.98. This was expected since the two models use the same incoming solar radiation forcing and the same albedo maps so the majority of the  $27 \text{ W m}^{-2}$  RMSD must be caused by the differences in the net longwave radiation  
20 estimation due to different LSTs, with DTD using MODIS LST and MIKE-SHE the modelled LST from the SW-ET module, and by the ground heat flux calculations.

#### 6.1.2 MIKE SHE vs. TSEB-2ART

The comparison of fluxes produced with MIKE SHE and TSEB-2ART follows a similar pattern as in the previous section, with low bias (maximum of  $22 \text{ W m}^{-2}$  in case of  $LE$ ) but also relatively low correlation and significant RMSD. However, the differences are  
25

smaller than in case of MIKE SHE–DTD comparison with RMSD and  $r$  for  $H$  and LE of  $63 \text{ W m}^{-2}$  and 0.52 and  $80 \text{ W m}^{-2}$  and 0.68 respectively. The correlation of EF is almost twice as high as in case of DTD, with a value of 0.40, and the characterization of AE is consistent between the two models with correlation of 0.95 and bias of  $28 \text{ W m}^{-2}$ , roughly half of which is caused by underestimation of net radiation and half of soil heat flux (not shown).

### 6.1.3 TSEB-2ART vs. DTD

The correlation between the turbulent fluxes modelled with TSEB-2ART and DTD is the highest of any model pairs, with correlation coefficient of 0.58 for  $H$  and 0.75 for LE, even though the fluxes were obtained at different hour of the day. The time offset is evident in the bias of AE, with the value of AE during the later Aqua overpass time being on average  $77 \text{ W m}^{-2}$  higher than the value of AE during Envisat overpass time. The biases are also present in the other flux estimates, particularly of LE with a value of  $58 \text{ W m}^{-2}$ . However, even though the biases are almost three times higher than in any other pair, the RMSD between TSEB-2ART and DTD estimated turbulent fluxes is comparable to RMSD of those fluxes between the other pairs. As can be seen from the split of the difference into systematic and unsystematic components, a large component of the MSD between the fluxes is systematic with  $\text{RMPD}_u$  reaching the lowest values of all the model pairs. The correlation and RMSD of EF is also the best of all the model pairs, with values of 0.43 and 0.15 respectively.

## 6.2 Temporal patterns

The results of comparing DTD and TSEB-2ART catchment wide evapotranspiration estimates against MIKE SHE are presented in Fig. 5 with the statistics summarized in Table 3. The correlation between the latent heat fluxes modelled with DTD or TSEB-2ART and MIKE SHE are quite similar with correlation coefficients having a value of 0.78 in case of comparing MIKE SHE and DTD and 0.82 in case of MIKE SHE and

TSEB-2ART. The biases between the modelled fluxes are quite small with the largest one present when looking at LE between MIKE SHE and TSEB-2ART and having a value of  $24 \text{ W m}^{-2}$  which represents just 10 % of the mean value of LE modelled by MIKE SHE. Both the remote sensing models have similar RMSD, between  $55 \text{ W m}^{-2}$  and  $60 \text{ W m}^{-2}$ , representing 24 % of the mean value of MIKE SHE LE.

## 7 Discussion

### 7.1 Spatial patterns

Even though DTD and TSEB-2ART estimate fluxes at different times during the day, the correlation between  $H$  and LE estimated by those two models is stronger than between either of the models and MIKE SHE. In addition the value of  $\text{RMPD}_u$  between  $H$  and LE estimated with those two models is lower than for the other comparisons, even though the RMSD between  $H$  and LE modelled with TSEB-2ART and MIKE SHE is lower. This indicates that the spatial patterns produced by the remotely sensed models have a stronger agreement with each other than with the patterns produced by the hydrological model. It can be presumed that if the DTD and TSEB-2ART estimated fluxes at the same time, the correlation would be even higher and the differences even smaller.

When the seasonal signal of the available energy is removed by replacing the turbulent fluxes by EF, the spatial patterns produced by the remote sensing models are still more strongly correlated than when either of them is compared to the hydrological model. The correlation coefficient of TSEB-2ART and DTD EF is 0.43 compared to the second highest value of 0.40 between MIKE SHE and TSEB-2ART EF. However, it should once again be kept in mind that the remote sensing models estimate the fluxes at different times of the day. Usually it is assumed that during clear sky days the EF remains constant throughout the daytime and especially around noon (Peng et al., 2013). However, by comparing the differences of EF modelled by MIKE SHE at

the Aqua and Envisat overpass times (Fig. 6), it can be seen that EF differs between the overpasses. This could be due to the fact that for the majority of the days used in this study there was some cloud cover over the Skjern river catchment (the threshold of inclusion in the study was 10 % of cloud free pixels during the night and day

5 Aqua overpass) meaning that it is highly probable that clouds have passed over the study pixels between the two satellite overpasses, breaking the assumption of self-preservation of EF (Crago, 1996). Therefore it can be assumed that if the EF from TSEB-2ART and DTD were estimated at the same time the correlation would be higher still.

10 When considering the causes of the remaining differences in the modelled fluxes, some factors can be directly removed. The three models used many of the same spatial datasets as input: LAI maps, land cover map and meteorological forcing data (air temperature, incoming solar radiation, humidity and wind speed). In addition DTD and MIKE SHE used the same albedo maps and MIKE SHE was calibrated using 15 the same Aqua MODIS LST observations as used by DTD. The mismatch caused by image misregistration was reduced by applying the median filter over the output maps, although on cloudy days there are many isolated pixels making the filtering less efficient. The available energy is very highly correlated in all the three comparisons, with small RMSD and bias in case of the two comparisons for which fluxes are 20 estimated at the same hour, so this is also not a major contributor to the differences between the turbulent fluxes. The largest differences regarding AE are found in TSEB-2ART, and are especially evident in the bias (Table 2). TSEB-2ART uses a totally different approach for estimating net radiation and radiation divergence, which is based 25 on 4SAIL RTM, as compared to the approaches of DTD and MIKE SHE, which are fundamentally based on the Beer–Lambert law. This also affects soil heat flux (G, results not shown) since net soil radiation participates in this process. Therefore, the difference in AE could be partly caused by the way that the different approaches model the transmission of energy through the canopy.

The remaining major causes of the observed differences in the model outputs could be: parametrization used in different land cover classes; the LST input maps estimated by different sensors, in case of DTD (MODIS) and TSEB-2ART (AATSR), or modelled, in case MIKE SHE; and the differences in the modelling approach between the three models even though all of them apply the two source modelling scheme.

### 7.1.1 Differences due to parameterization of land cover classes

Figures 7–9 show boxplots of the turbulent fluxes, AE and EF split according to the land cover class. The graphs indicate that the statistical distribution of fluxes in the different land cover classes is quite similar among the models, albeit with a large number of outlier points in sensible heat estimations of all models and latent heat estimations of DTD. This is despite DTD and TSEB-2ART sharing more common land cover class dependent parameters with each other than with MIKE SHE (Table 1). When looking at the median and 25th and 75th percentile values of evapotranspiration the largest differences between MIKE SHE and the remote sensing models occur in conifer forest in case of DTD and in croplands and grasslands in case of TSEB-2ART. However, those differences do not appear as significant in the case of DTD as could be expected from the results shown in Table 2. On the other hand, the larger differences found for LE in crops and grass between TSEB-2ART and MIKE SHE are definitely reflected in a total bias of  $22 \text{ W m}^{-2}$  (Table 2). The fact that these differences are evident in grass and crops is again due to the different radiation scheme of TSEB-2ART. Firstly, TSEB-2ART estimates the albedo based on the spectral properties of the leaves and soil whereas DTD and MIKE SHE use the albedo derived from MODIS reflectances. Secondly, TSEB-2ART is also able to account for different leaf inclinations distribution functions. Grass and cereal crops are characterised by a more erectophyll leaf distribution than the spherical distribution characteristic of other vegetation types, such as conifers and some broadleaved forest or shrubs, and implemented in the DTD and MIKE SHE. It is also interesting to note in Fig. 9 that although the boxes for  $H$  are larger for DTD and the boxes for LE have similar size, the range between the 25th and 75th percentiles is

[Title Page](#)[Abstract](#)[Introduction](#)[Conclusions](#)[References](#)[Tables](#)[Figures](#)[◀](#)[▶](#)[◀](#)[▶](#)[Back](#)[Close](#)[Full Screen / Esc](#)[Printer-friendly Version](#)[Interactive Discussion](#)

larger for TSEB-2ART when looking at EF, meaning it has larger spread. This is due to the fact that TSEB-2ART shows a larger variability in AE than DTD, which is influencing the calculation of EF.

### 7.1.2 Differences due to estimates of LST and its component temperatures

5 Table 4 shows the statistical comparison between the LST, which is used as input of the remote sensing models and is one of the outputs of the hydrological model, for all the pixels where flux comparison was also performed. The graphical representation is shown in top left panels of Figs. 10–12. When comparing LST it must be noted that it is dependent on the viewing geometry, such as VZA, which is quite different  
10 between the two satellites and also between the satellites and the hydrological model, for which the sensor is assumed to be directly at nadir. The correlation between the LST from the different model pairs is quite high, with  $r$  around 0.9 when comparing the remotely sensed LST from MODIS and AATSR with the MIKE SHE estimates but reaching 0.97 when the two remotely sensed LSTs are compared. RMSD of LST is  
15 quite high, between 4 and 5 °C in case of comparing MODIS and AATSR to MIKE SHE and around of 3 °C when comparing MODIS with AATSR, although in this case the time difference between the observations should be kept in mind.

Although the high spatial correlation of LST would indicate that the different sources of LST are not a major component in the discrepancies between the modelled fluxes  
20 it must be noted that the fluxes are strongly dependent on the LST– $T_a$  gradient and that this dependency is non-linear due to the turbulent transport of heat between the surface and the overlying air (Obukhov, 1971). Due to this non-linearity, the systematic differences in LST between models can potentially lead to larger unsystematic differences in flux estimations. An additional complication in the current study is the fact  
25 the DTD uses the relative temperature difference between night and day observations (Guzinski et al., 2013) and TSEB-2ART is based on the differences of temperature between the nadir and forward LST observations (Nieto et al., 2013) for flux estimation. It is also interesting to note that although MIKE SHE was calibrated with MODIS

<a href="#">Title Page</a>	
<a href="#">Abstract</a>	<a href="#">Introduction</a>
<a href="#">Conclusions</a>	<a href="#">References</a>
<a href="#">Tables</a>	<a href="#">Figures</a>
<a href="#">◀</a>	<a href="#">▶</a>
<a href="#">◀</a>	<a href="#">▶</a>
<a href="#">Back</a>	<a href="#">Close</a>
<a href="#">Full Screen / Esc</a>	
<a href="#">Printer-friendly Version</a>	
<a href="#">Interactive Discussion</a>	

Aqua LST observations in the Skjern river catchment, the two satellite based LSTs have a better agreement each other than with MIKE SHE, despite the overpass times of the two satellites being different. This indicates that the use of LST observations from a satellite sensor, either as a forcing input for MIKE SHE model or for data assimilation (in addition to it being used for calibration), could potentially improve the spatial performance of the hydrological model.

In addition, the canopy, soil and in-canopy air temperatures ( $T_C$ ,  $T_S$  and  $T_{AC}$  respectively) estimated by the different models are also compared in Table 4. Estimation of those temperatures could be considered as an intermediate step during the estimation of the fluxes in the models (Norman et al., 1995; Overgaard and Rosbjerg, 2005), thereby allowing a deeper understanding of the internal model behaviour. The three models apply different methods for estimating those temperatures. In case of DTD, temperatures are not used directly during the flux estimation (the time differential temperature observations are used) but are derived as a final step when all the flux and resistance values are already established using rearranged Eqs. (A27), (A29) and (A33) from Guzinski et al. (2014). TSEB-2ART uses the viewing geometry of the two observation angles within a radiative transfer model framework to estimate  $T_C$  and  $T_S$  which, together with the resistances to heat transport, are then used to calculate  $T_{AC}$  and the fluxes using the TSEB formulations (Nieto et al., 2013; Norman et al., 1995). In MIKE SHE the temperatures, together with humidity, are derived by solving a set of 10 linear equations involving the resistances and AE as parameters, after which the turbulent fluxes are derived (Overgaard and Rosbjerg, 2005).

Despite those three different methods the correlation between the temperatures is quite high (Table 4) which is surprising considering the much lower correlation between the modelled turbulent fluxes. Again, this is probably caused by the non-linearity between the gradient of temperatures and the heat flux due to turbulence. It could also be due to the heating effect that the interaction between soil temperature and heat fluxes produces for the temperature of the air at the canopy interface, when

[Title Page](#)[Abstract](#)[Introduction](#)[Conclusions](#)[References](#)[Tables](#)[Figures](#)[◀](#)[▶](#)[◀](#)[▶](#)[Back](#)[Close](#)[Full Screen / Esc](#)[Printer-friendly Version](#)[Interactive Discussion](#)

the resistances are configured in series. The highest correlation, above 0.9 for all the pairs, is for  $T_{AC}$ , and the lowest, ranging from 0.67 to 0.82, is for  $T_S$ . Overall the two remote sensing models have most similar spatial patterns of  $T_S$ , and MIKE SHE and DTD have most similar spatial patterns for the other temperatures.

Furthermore, since TSEB-2ART model relies on the differences observed between the nadir and forward LST of AATSR in order to derive  $T_C$  and  $T_S$ , it is sensitive to errors in the estimation of LST at the two viewing angles. Those errors might be significant if, for example, atmospheric water vapour is not properly characterized and accounted for, due to the different optical path lengths between the forward (VZA = 55°) and the nadir observation. Since the atmospheric path length of the forward view is longer, the a priori uncertainty in the estimation of forward LST is higher than in case of nadir LST. In Figs. 11 and 12 it can be seen that this occurs in a number of cases, mostly leading to severe underestimation of  $T_C$  and  $T_{AC}$  and overestimation of  $T_S$ . This large bias in TSEB-2ART estimated  $T_C$  is also present in the statistical comparison in Table 4. It also appears that MIKE SHE overestimates high values of  $T_C$  (Figs. 10 and 11) although this overestimation is not severe. The overestimation of  $T_C$  is reflected in MIKE SHE LST scatter plots, which indicates that it happens at high LAI values when vegetation cover fraction is close to 1.

### 7.1.3 Differences due to modelling approach

Although there are differences in the estimated temperatures that could lead to larger unsystematic differences in the fluxes estimates, it is likely that there are also other factors contributing to the inconsistencies between fluxes. One of the factors could be the methodology employed by the different models for splitting of the available energy into the sensible and latent heat fluxes and in particular the way they estimate the resistances to heat and moisture transport. The two remote sensing models ensure the land surface energy balance by calculating latent heat flux as the residual of the other fluxes, i.e.  $LE = AE - H$  (Norman et al., 1995). The hydrological model, on the other hand, derives the latent and sensible heat fluxes concurrently (Overgaard and

[Title Page](#)

[Abstract](#)

[Introduction](#)

[Conclusions](#)

[References](#)

[Tables](#)

[Figures](#)

◀

▶

◀

▶

[Back](#)

[Close](#)

[Full Screen / Esc](#)

[Printer-friendly Version](#)

[Interactive Discussion](#)

Rosbjerg, 2005). In addition the resistance network for LE in MIKE SHE has two extra resistance components compared to the resistance network for H: the resistance to soil evaporation and the stomata resistance to transpiration. Both of them depend on the soil moisture as modelled by the hydrological component of MIKE SHE. If the spatial

5 patterns of the soil moisture estimated with MIKE SHE do not correspond closely to the spatial patterns seen by the satellites this could lead to the different spatial patterns of the estimated fluxes.

Finally, Fig. 13 illustrates the effect of modifying the  $R_S$  formulation in the DTD, as proposed in Eq. (4). The  $R_S$  values estimated with DTD and TSEB-2ART are 10 compared for all the pixels where the flux comparison was performed. In this case, the TSEB-2ART derived  $R_S$  can be thought of as the “true” value, since it uses the original  $R_S$  equation (Eq. 3), with  $T_S$  and  $T_C$  derived directly through the inversion of the RTM. The overestimation of  $R_S$  by DTD, visible in the left panel for TSEB- 15 2ART  $R_S$  values between 100 and 200  $\text{s m}^{-1}$ , is due to misparametrization of the differences between the canopy and soil temperatures in the original DTD formulation and is mostly present in the coniferous forest. In the right panel this overestimation is less pronounced, indicating that the new  $R_S$  equation is better at parametrizing this temperature difference. The correlation parameter between the two resistances has increased from 0.63 in case of the old formulation to 0.71 in case of the new one, while 20 the RMSD has decreased by around 15 % from 37 to 32  $\text{s m}^{-1}$ .

## 7.2 Temporal patterns

Both remote sensing models are reasonably accurate in matching MIKE SHE 25 catchment wide estimates of evapotranspiration, with the seasonal curve clearly visible for both models (Fig. 5) and reflecting the MIKE SHE seasonality well. The DTD model overestimates the fluxes slightly during the winter months and underestimates in spring. On the other hand TSEB-2ART underestimates throughout the year. This is probably due to the underestimation of AE by this model (see Table 2) which is mostly assigned to LE as it is calculated as a residual of the surface energy balance.

The figure also highlights another weakness of the remote sensing models, namely that they only produce results on clear sky days. The great majority of latent heat fluxes estimated by the remote sensing models, and by the hydrological model on the same dates as the remote sensing models, lie above the line representing the smoothed, 7 year averaged flux for each day of year. This is because in the Skjern river environment the evapotranspiration is mainly driven by availability of energy (and not of water), and therefore on clear sky days the evapotranspiration will be higher than average. This has to be taken into account when extrapolating temporal patterns of evapotranspiration derived purely by the remote sensing input based models.

10 There are a couple of cases where the clear sky evapotranspiration modelled by  
MIKE SHE is much below the average line, even though the remote sensing models  
estimate much higher latent heat fluxes on those days. This most probably corresponds  
to days with soil drier than normal and could indicate: (1) a problem of the hydrological  
model in estimating the moisture of the upper layer of the soil or of the root zone  
15 during dry conditions, or (2) be related to uncertainties in the interpolated rainfall data  
due to omission by the rain gauges of local convective rainfall during the summer  
period. Some of the latent heat fluxes estimated by TSEB-2ART during the spring  
are also below the average line and this is caused by the general underestimation of  
evapotranspiration by this model.

## 20 8 Conclusions and outlook

Two remote sensing models and one hydrological model were run over an area covering a river catchment in western Denmark and the spatial and temporal patterns of the modelled evapotranspiration were compared. The spatial patterns of latent and sensible heat fluxes as well as EF produced by the remote sensing models were more strongly correlated with each other than the patterns produced by either of the remote sensing models compared to the hydrological model. This was the case even though the remote sensing models estimated the fluxes at different hour of the day,

Title Page	
Abstract	Introduction
onclusions	References
Tables	Figures
◀	▶
◀	▶
Back	Close
Full Screen / Esc	
Printer-friendly Version	
Interactive Discussion	

due to different satellites being used for LST estimates. At the same time, the temporal patterns of evapotranspiration produced by both of the remote sensing models and the hydrological model were strongly correlated, with small RMSD and small bias. Those observations would appear to support the hypothesis, that the remote sensing models

5 would better represent the spatial patterns of evapotranspiration present throughout the catchment while the hydrological model would better represent the catchment wide evapotranspiration.

This points towards a possibility of using the remotely sensed evapotranspiration to improve the spatial accuracy of distributed, physically-based hydrological models.

10 This could be achieved either through using the estimated latent heat flux as one of the calibrating parameters or through data assimilation during the model run. Certain attempts at incorporating spatial distributed data derived through remote sensing into hydrological models, either through data assimilation or calibration, have already been

15 made but they were mostly focused on soil moisture (e.g. Draper et al., 2011; Corato et al., 2013), LST (Stisen et al., 2011a; Ridler et al., 2012) or LAI (Boegh et al., 2004). Pipunic et al. (2008) have looked at assimilating simulated  $H$  and LE estimates into a land surface model, however this was done with a one-dimensional single column model, i.e. without considering spatial patterns. Others have assimilated ET maps into distributed hydrological models but the impact of that assimilation was inconclusive

20 (Pan et al., 2008; Schuurmans et al., 2011). Therefore, further studies are needed to establish whether ET, and in particular its spatial distribution, would bring any additional information beyond what is provided by soil moisture or LST estimates alone. In the case of MIKE SHE it might also be useful to use the  $T_C$ ,  $T_S$  and  $T_{AC}$  estimates from the remote sensing models to constrain the number of unknowns that need to be

25 addressed in the model. Methodologies for validating the accuracy of spatial patterns at the catchment scale, while at the same time remaining independent of the model used, would also have to be investigated.

*Acknowledgements.* The work has been carried out under the HOBE project funded by the VILLUM FOUNDATION.

[Title Page](#)

[Abstract](#)

[Introduction](#)

[Conclusions](#)

[References](#)

[Tables](#)

[Figures](#)

[◀](#)

[▶](#)

[◀](#)

[▶](#)

[Back](#)

[Close](#)

[Full Screen / Esc](#)

[Printer-friendly Version](#)

[Interactive Discussion](#)

**Inter-comparison of energy balance and hydrological models over a whole river catchment**

R. Guzinski et al.

Anderson, M. C., Allen, R. G., Morse, A., and Kustas, W. P.: Use of Landsat thermal imagery in monitoring evapotranspiration and managing water resources, *Remote Sens. Environ.*, 122, 50–65, 2012. 5907

5 Barker, F., Soh, Y., and Evans, R.: Properties of the geometric mean functional relationship, *Biometrics*, 44, 279–281, 1988. 5918

Boegh, E., Thorsen, M., Butts, M., Hansen, S., Christiansen, J., Abrahamsen, P., Hasager, C., Jensen, N., van der Keur, P., Refsgaard, J., Schelde, K., Soegaard, H., and Thomsen, A.: Incorporating remote sensing data in physically based distributed agro-hydrological modelling, *J. Hydrol.*, 287, 279–299, doi:10.1016/j.jhydrol.2003.10.018, 2004. 5930

10 Boegh, E., Poulsen, R., Butts, M., Abrahamsen, P., Dellwik, E., Hansen, S., Hasager, C. B., Ibrom, A., Loerup, J.-K., Pilegaard, K., and Soegaard, H.: Remote sensing based evapotranspiration and runoff modeling of agricultural, forest and urban flux sites in Denmark: from field to macro-scale, *J. Hydrol.*, 377, 300–316, 2009. 5911

15 Campbell, G. and Norman, J.: *Introduction to Environmental Biophysics*, Springer, New York, New York, USA, 1998. 5907

Conradt, T., Wechsung, F., and Bronstert, A.: Three perceptions of the evapotranspiration landscape: comparing spatial patterns from a distributed hydrological model, remotely sensed surface temperatures, and sub-basin water balances, *Hydrol. Earth Syst. Sci.*, 17, 2947–2966, doi:10.5194/hess-17-2947-2013, 2013. 5907

20 Corato, G., Matgen, P., Giustarini, L., and Fenicia, F.: On the effects of hydrological model structure on soil moisture data assimilation, *EGU General Assembly*, 7–12 April 2013, Vienna, Austria, EGU2013-11602, 2013. 5930

Crago, R. D.: Conservation and variability of the evaporative fraction during the daytime, *J. Hydrol.*, 180, 173–194, doi:10.1016/0022-1694(95)02903-6, 1996. 5923

25 Donlon, C., Berruti, B., Buongiorno, A., Ferreira, M.-H., Féminias, P., Frerick, J., Goryl, P., Klein, U., Laur, H., Mavrocordatos, C., Nieke, J., Rebhan, H., Seitz, B., Stroede, J., and Sciarra, R.: The global monitoring for environment and security (GMES) sentinel-3 mission, *Remote Sens. Environ.*, 120, 37–57, 2012. 5917

30 Draper, C., Mahfouf, J.-F., Calvet, J.-C., Martin, E., and Wagner, W.: Assimilation of ASCAT near-surface soil moisture into the SIM hydrological model over France, *Hydrol. Earth Syst. Sci.*, 15, 3829–3841, doi:10.5194/hess-15-3829-2011, 2011. 5930

<a href="#">Title Page</a>	
<a href="#">Abstract</a>	<a href="#">Introduction</a>
<a href="#">Conclusions</a>	<a href="#">References</a>
<a href="#">Tables</a>	<a href="#">Figures</a>
<a href="#">◀</a>	<a href="#">▶</a>
<a href="#">◀</a>	<a href="#">▶</a>
<a href="#">Back</a>	<a href="#">Close</a>
<a href="#">Full Screen / Esc</a>	
<a href="#">Printer-friendly Version</a>	
<a href="#">Interactive Discussion</a>	

Graham, D. N. and Butts, M. B.: Flexible, integrated watershed modelling with MIKE SHE, in: Watershed Models, edited by: Singh, V. P. and Frevert, D. K., Taylor and Francis Group, Boca Raton, FL, USA, 245–272, 2005. 5909

5 Greve, M. H., Greve, M. B., Bøcher, P. K., Balstrøm, T., Breuning-Madsen, H., and Krogh, L.: Generating a Danish raster-based topsoil property map combining choropleth maps and point information, *Geogr. Tidsskr.*, 107, 1–12, 2007. 5913

10 Guzinski, R., Anderson, M. C., Kustas, W. P., Nieto, H., and Sandholt, I.: Using a thermal-based two source energy balance model with time-differencing to estimate surface energy fluxes with day–night MODIS observations, *Hydrol. Earth Syst. Sci.*, 17, 2809–2825, doi:10.5194/hess-17-2809-2013, 2013. 5910, 5914, 5916, 5925

Guzinski, R., Nieto, H., Jensen, R., and Mendiguren, G.: Remotely sensed land-surface energy fluxes at sub-field scale in heterogeneous agricultural landscape and coniferous plantation, *Biogeosciences Discuss.*, 11, 4857–4908, doi:10.5194/bgd-11-4857-2014, 2014. 5914, 5926

15 Jensen, K. H. and Illangasekare, T. H.: HOBE: a hydrological observatory, *Vadose Zone J.*, 10, 1–7, 2011. 5910, 5911

Ji, L. and Gallo, K.: An agreement coefficient for image comparison, *Photogramm. Eng. Rem. S.*, 72, 823–833, 2006. 5910, 5918, 5919

20 Ji, L., Gallo, K., Eidenshink, J., and Dwyer, J.: Agreement evaluation of AVHRR and MODIS 16-day composite NDVI data sets, *Int. J. Remote Sens.*, 29, 4839–4861, 2008. 5919

Jiang, L. and Islam, S.: Estimation of surface evaporation map over Southern Great Plains using remote sensing data, *Water Resour. Res.*, 37, 329–340, doi:10.1029/2000WR900255, 2001. 5908

25 Kalma, J. D., McVicar, T. R., and McCabe, M. F.: Estimating land surface evaporation: a review of methods using remotely sensed surface temperature data, *Surv. Geophys.*, 29, 421–469, 2008. 5908

Kustas, W. P. and Goodrich, D. C.: Special section – Monsoon 90 Multidisciplinary Experiment – preface, *Water Resour. Res.*, 30, 1211–1225, 1994. 5915

30 Kustas, W. P. and Norman, J. M.: A two-source approach for estimating turbulent fluxes using multiple angle thermal infrared observations, *Water Resour. Res.*, 33, 1495–1508, 1997. 5916

## Inter-comparison of energy balance and hydrological models over a whole river catchment

R. Guzinski et al.

[Title Page](#)

[Abstract](#)

[Introduction](#)

[Conclusions](#)

[References](#)

[Tables](#)

[Figures](#)

◀

▶

◀

▶

[Back](#)

[Close](#)

[Full Screen / Esc](#)

[Printer-friendly Version](#)

[Interactive Discussion](#)

Kustas, W. P. and Norman, J. M.: Evaluation of soil and vegetation heat flux predictions using a simple two-source model with radiometric temperatures for partial canopy cover, *Agr. Forest Meteorol.*, 94, 13–29, 1999. 5915, 5916

Liang, S.: Narrowband to broadband conversions of land surface albedo I: Algorithms, *Remote Sens. Environ.*, 76, 213–238, 2001. 5911

Nieto, H., Guzinski, R., Jensen, R., Sandholt, I., and Jensen, K.: TSEBRTM: Coupling a canopy Radiative Transfer model with a Two Source Energy Balance Model for the Estimation of Surface Energy Fluxes with Dual-Angle Land Surface Temperature, TR32-HOBE International Symposium, 11–14 March 2013, Bonn, Germany, S4-128, available at: [http://tr32meeting.uni-koeln.de/images/abstract/s4/TR32-HOBE-S4-Thursday-1140-1200\\_Nieto.pdf](http://tr32meeting.uni-koeln.de/images/abstract/s4/TR32-HOBE-S4-Thursday-1140-1200_Nieto.pdf), last access: 27 May 2014, 2013. 5910, 5916, 5925, 5926

Norman, J. M., Kustas, W. P., and Humes, K. S.: Source approach for estimating soil and vegetation energy fluxes in observations of directional radiometric surface temperature, *Agr. Forest Meteorol.*, 77, 263–293, 1995. 5909, 5913, 5914, 5916, 5926, 5927

Norman, J. M., Kustas, W., Prueger, J., and Diak, G.: Surface flux estimation using radiometric temperature: a dual-temperature-difference method to minimize measurement errors, *Water Resour. Res.*, 36, 2263–2274, 2000. 5910, 5914, 5915, 5951

Obukhov, A.: Turbulence in an atmosphere with a non-uniform temperature, *Bound.-Lay. Meteorol.*, 2, 7–29, 1971. 5925

Overgaard, J. and Rosbjerg, D.: Energy-Based Land-Surface Modelling: New Opportunities in Integrated Hydrological Modelling, Technical University of Denmark – Danmarks Tekniske Universitet, Department of Hydrodynamics and Water Resourceres – Strømningsmekanik og Vandressourcer, Copenhagen, Denmark, 2005. 5912, 5926, 5927

Pan, M., Wood, E. F., Wójcik, R., and McCabe, M. F.: Estimation of regional terrestrial water cycle using multi-sensor remote sensing observations and data assimilation, *Remote Sens. Environ.*, 112, 1282–1294, doi:10.1016/j.rse.2007.02.039, 2008. 5907, 5930

Peng, J., Borsche, M., Liu, Y., and Loew, A.: How representative are instantaneous evaporative fraction measurements of daytime fluxes?, *Hydrol. Earth Syst. Sci.*, 17, 3913–3919, doi:10.5194/hess-17-3913-2013, 2013. 5918, 5922

Pipunic, R., Walker, J., and Western, A.: Assimilation of remotely sensed data for improved latent and sensible heat flux prediction: a comparative synthetic study, *Remote Sens. Environ.*, 112, 1295–1305, doi:10.1016/j.rse.2007.02.038, 2008. 5930

Refsgaard, J. C.: Parameterisation, calibration and validation of distributed hydrological models, *J. Hydrol.*, 198, 69–97, 1997. 5909

Ridder, M. E., Sandholt, I., Butts, M., Lerer, S., Mougin, E., Timouk, F., Kerfoot, L., and Madsen, H.: Calibrating a soil–vegetation–atmosphere transfer model with remote sensing estimates of surface temperature and soil surface moisture in a semi arid environment, *J. Hydrol.*, 436–437, 1–12, doi:10.1016/j.jhydrol.2012.01.047, 2012. 5930

5 Schuurmans, J. M., van Geer, F. C., and Bierkens, M. F. P.: Remotely sensed latent heat fluxes for model error diagnosis: a case study, *Hydrol. Earth Syst. Sci.*, 15, 759–769, doi:10.5194/hess-15-759-2011, 2011. 5908, 5930

10 Shuttleworth, W. J. and Wallace, J.: Evaporation from sparse crops—an energy combination theory, *Q. J. Roy. Meteor. Soc.*, 111, 839–855, 1985. 5912

Stisen, S., Sandholt, I., Nørgaard, A., Fensholt, R., and Jensen, K. H.: Combining the triangle method with thermal inertia to estimate regional evapotranspiration, applied to MSG-SEVIRI data in the Senegal River basin, *Remote Sens. Environ.*, 112, 1242–1255, 2008. 5908

15 Stisen, S., McCabe, M. F., Refsgaard, J. C., Lerer, S., and Butts, M. B.: Model parameter analysis using remotely sensed pattern information in a multi-constraint framework, *J. Hydrol.*, 409, 337–349, 2011a. 5909, 5911, 5912, 5913, 5930

Stisen, S., Sonnenborg, T. O., Højberg, A. L., Troldborg, L., and Refsgaard, J. C.: Evaluation of 20 climate input biases and water balance issues using a coupled surface–subsurface model, *Vadose Zone J.*, 10, 37–53, 2011b. 5911

Su, Z.: The Surface Energy Balance System (SEBS) for estimation of turbulent heat fluxes, *Hydrol. Earth Syst. Sci.*, 6, 85–100, doi:10.5194/hess-6-85-2002, 2002. 5909

Verhoef, W., Jia, L., Xiao, Q., and Su, Z.: Unified optical-thermal four-stream radiative transfer theory for homogeneous vegetation canopies, *IEEE T. Geosci. Remote*, 45, 1808–1822, 25 2007. 5916

## Inter-comparison of energy balance and hydrological models over a whole river catchment

R. Guzinski et al.

[Title Page](#)

[Abstract](#)

[Introduction](#)

[Conclusions](#)

[References](#)

[Tables](#)

[Figures](#)

◀

▶

◀

▶

[Back](#)

[Close](#)

[Full Screen / Esc](#)

[Printer-friendly Version](#)

[Interactive Discussion](#)



## Inter-comparison of energy balance and hydrological models over a whole river catchment

R. Guzinski et al.

**Table 1.** Land cover dependent parameters for the three models. The equations referred to in the table are Eq. (a):  $0.14 \cdot \text{LAI} + 0.09$  and Eq. (b):  $0.12 \cdot \text{LAI} + 0.07$  where LAI is leaf area index. In case of DTD the grass and crop vegetation heights are scaled linearly from 0.1 to the indicated value, also based on LAI.

Parameter	Land cover class												Units
	Grass			Coniferous Forest			Heath			Crop			
	MIKE SHE	DTD	TSEB-2ART	MIKE SHE	DTD	TSEB-2ART	MIKE SHE	DTD	TSEB-2ART	MIKE SHE	DTD	TSEB-2ART	
Vegetation height ( $h_c$ )	Eq. (a)	0.3	0.3	Eq. (a)	20.0	20.0	Eq. (a)	1.0	1.0	Eq. (a)	0.8	0.8	m
Clumping factor	N/A	1.0	N/A	N/A	0.5	N/A	N/A	0.9	N/A	N/A	0.9	N/A	unitless
Canopy height/canopy width	N/A	1.0	1.0	N/A	3.0	3.0	N/A	1.0	1.0	N/A	1.0	1.0	unitless
Leaf size	0.02	0.01	0.01	0.02	0.01	0.01	0.02	0.01	0.01	0.02	0.01	0.01	m
Temperature measurement height	$h_c + 2$	$h_c + 2$	$h_c + 2$	$h_c + 2$	$h_c + 2$	$h_c + 2$	$h_c + 2$	$h_c + 2$	$h_c + 2$	$h_c + 2$	$h_c + 2$	$h_c + 2$	m
Wind measurement height	$h_c + 10$	$h_c + 10$	$h_c + 10$	$h_c + 10$	$h_c + 10$	$h_c + 10$	$h_c + 10$	$h_c + 10$	$h_c + 10$	$h_c + 10$	$h_c + 10$	$h_c + 10$	m
Root depth	Eq. (b)	N/A	N/A	Eq. (b)	N/A	N/A	Eq. (b)	N/A	N/A	Eq. (b)	N/A	N/A	m
Minimum stomata resistance	90	N/A	N/A	150	N/A	N/A	120	N/A	N/A	90	N/A	N/A	$\text{s m}^{-1}$
Extinction coefficient	0.6	N/A	N/A	0.5	N/A	N/A	0.3	N/A	N/A	0.6	N/A	N/A	unitless

<a href="#">Title Page</a>	<a href="#">Abstract</a>	<a href="#">Introduction</a>
<a href="#">Conclusions</a>	<a href="#">References</a>	
<a href="#">Tables</a>	<a href="#">Figures</a>	
<a href="#">◀</a>	<a href="#">▶</a>	
<a href="#">◀</a>	<a href="#">▶</a>	
<a href="#">Back</a>	<a href="#">Close</a>	
<a href="#">Full Screen / Esc</a>		
<a href="#">Printer-friendly Version</a>		
<a href="#">Interactive Discussion</a>		

## Inter-comparison of energy balance and hydrological models over a whole river catchment

R. Guzinski et al.

**Table 2.** Statistical comparison between MIKE SHE, DTD and TSEB-2ART models for sensible and latent heat fluxes (H and LE), available energy (AE) and evaporative fraction (EF). Statistics used: correlation coefficient ( $r$ ), Root Mean Square Difference (RMSD), systematic and unsystematic Root Mean Product Differences (RMPD<sub>s</sub> and RMPD<sub>u</sub> respectively), the percentage of Mean Square Difference (MSD) attributed to systematic and unsystematic Mean Product Differences (MPD) (MPD<sub>s</sub>/MSD and MPD<sub>u</sub>/MSD respectively) and bias. The statistics for H, LE and AE are in  $\text{W m}^{-2}$  with the exception of MPD<sub>s</sub>/MSD and MPD<sub>u</sub>/MSD which are percentages. The statistics for EF are unitless with the exception of MPD<sub>s</sub>/MSD and MPD<sub>u</sub>/MSD which are percentages.

		$r$	RMSD	RMPD <sub>s</sub>	RMPD <sub>u</sub>	MPD <sub>s</sub> /MSD	MPD <sub>u</sub> /MSD	Bias
MIKE SHE-DTD	H	0.43	78	13	77	3	97	-4
	LE	0.54	97	21	95	5	95	-9
	AE	0.98	27	15	23	31	69	-12
	EF	0.21	0.19	0.04	0.19	4	96	-0.01
MIKE SHE-TSEB-2ART	H	0.52	63	20	59	11	89	7
	LE	0.68	80	25	76	10	90	22
	AE	0.95	44	28	34	40	60	28
	EF	0.40	0.17	0.03	0.17	3	97	0.01
TSEB-2ART-DTD	H	0.58	59	25	53	18	82	-20
	LE	0.75	86	58	63	46	54	-58
	AE	0.94	85	77	36	82	18	-77
	EF	0.43	0.15	0.04	0.15	6	94	-0.04

		<i>r</i>	RMSD	%RMSD	Bias	%Bias
MIKE SHE-DTD	LE	0.78	59	24	-2	-1
MIKE SHE-TSEB-2ART	LE	0.82	55	24	24	10

**Table 3.** Statistical comparison of catchment wide latent heat fluxes modelled by the model pairs (MIKE SHE–DTD and MIKE SHE–TSEB-2ART) for predominantly cloud free days over the period of 7 years. Statistics used: correlation coefficient ( $r$ ), Root Mean Square Difference (RMSD), relative RMSD (%RMSD), bias and relative bias (%bias). RMSD and bias are in  $\text{W m}^{-2}$  while %RMSD and %Bias are calculated as the statistic divided by the mean of the MIKE SHE LE estimates and are percentages.

## Title Page

## Abstract

## Introduction

## Conclusions

## References

## Tables

## Figures

18

1

Back

Close

Full Screen / Esc

Interactive Discussion

## Inter-comparison of energy balance and hydrological models over a whole river catchment

R. Guzinski et al.

**Table 4.** Statistical comparison between MIKE SHE, DTD and TSEB-2ART models for the land surface temperatures (LST), canopy temperatures ( $T_C$ ), soil temperatures ( $T_S$ ) and in-canopy air temperatures ( $T_{AC}$ ). Statistics used: correlation coefficient ( $r$ ), Root Mean Square Difference (RMSD), systematic and unsystematic Root Mean Product Differences (RMPD<sub>s</sub> and RMPD<sub>u</sub> respectively), the percentage of Mean Square Difference (MSD) attributed to systematic and unsystematic Mean Product Differences (MPD) (MPD<sub>s</sub>/MSD and MPD<sub>u</sub>/MSD respectively) and bias. LST comes from Aqua MODIS observations in case of DTD, nadir view Envisat AATSR observations in case of TSEB-2ART and is modelled in case of MIKE SHE. The other temperatures are estimated by all models. The statistics are in °C with the exception of MPD<sub>s</sub>/MSD and MPD<sub>u</sub>/MSD which are percentages.

		$r$	RMSD	RMPD <sub>s</sub>	RMPD <sub>u</sub>	MPD <sub>s</sub> /MSD	MPD <sub>u</sub> /MSD	Bias
MIKE SHE–DTD	LST	0.89	4.2	2.8	3.2	43	57	2.8
	$T_C$	0.91	3.2	1.7	2.7	27	73	1.6
	$T_S$	0.67	8.0	4.9	6.3	38	62	-3.7
	$T_{AC}$	0.95	2.2	1.0	2.0	19	81	1.0
MIKE SHE–TSEB-2ART	LST	0.91	5.0	4.1	2.9	67	33	4.0
	$T_C$	0.78	11.6	10.3	5.4	78	22	9.5
	$T_S$	0.75	7.1	4.4	5.6	39	61	-2.1
	$T_{AC}$	0.90	7.1	6.3	3.2	79	21	6.0
TSEB-2ART–DTD	LST	0.97	2.9	2.3	1.8	61	39	-2.1
	$T_C$	0.85	10.5	9.6	4.4	83	17	-8.6
	$T_S$	0.82	6.5	2.8	5.9	19	81	-2.8
	$T_{AC}$	0.93	6.8	6.2	2.7	84	16	-5.9

<a href="#">Title Page</a>	<a href="#">Abstract</a>	<a href="#">Introduction</a>
<a href="#">Conclusions</a>	<a href="#">References</a>	
<a href="#">Tables</a>	<a href="#">Figures</a>	
<a href="#">◀</a>	<a href="#">▶</a>	
<a href="#">◀</a>	<a href="#">▶</a>	
<a href="#">Back</a>	<a href="#">Close</a>	
<a href="#">Full Screen / Esc</a>		

[Printer-friendly Version](#)

[Interactive Discussion](#)

## Inter-comparison of energy balance and hydrological models over a whole river catchment

R. Guzinski et al.

## Title Page

## Abstract

## Introduction

## Conclusions

## References

## Tables

## Figures

100

10 of 10

Page 10

Page 10

— 1 —

84

Page 10

Page 10 of 10

Page 1 of 1

Chap. 10: Diagrams

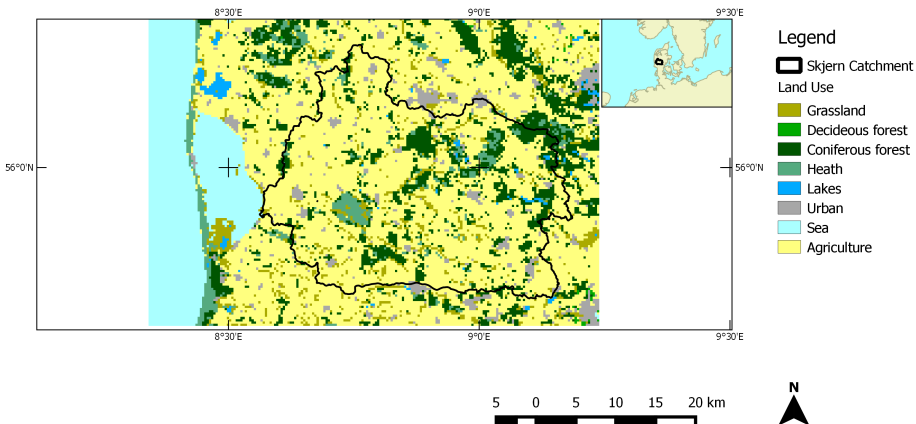


**Figure 1.** Land use map of the study area: the Skjern river catchment in the west of Denmark's Jutland peninsula.

**Inter-comparison of energy balance and hydrological models over a whole river catchment**

R. Guzinski et al.

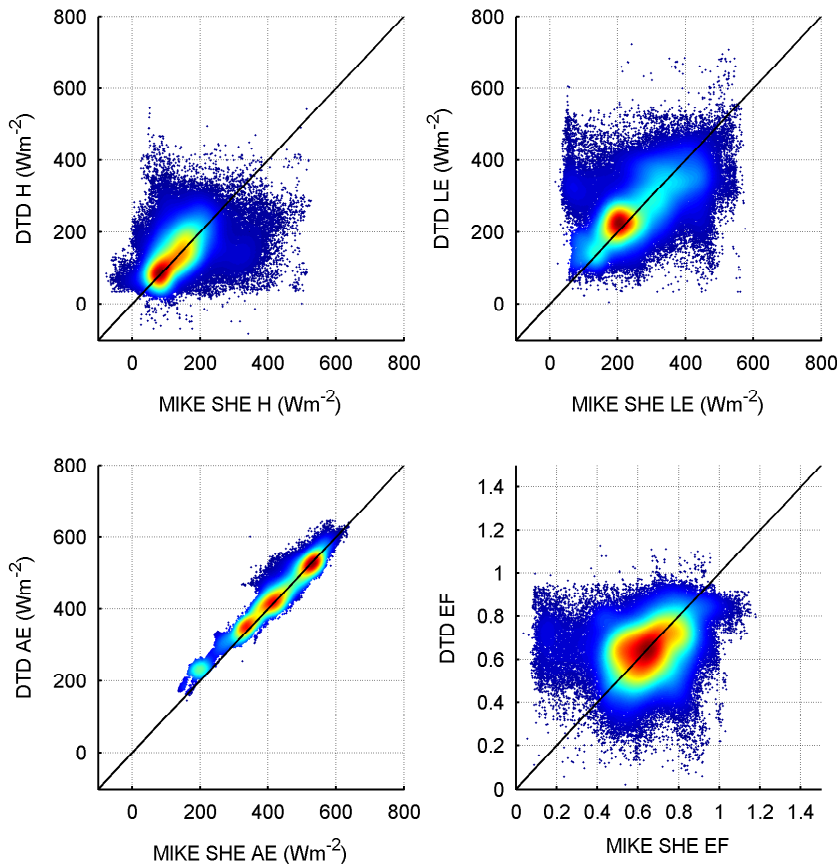


**Figure 2.** Density scatter plot of over 105 000 points comparing the sensible heat flux (top left), latent heat flux (top right), available energy (bottom left) and evaporative fraction (bottom right) modelled by MIKE SHE and DTD. Red colour indicates higher density of points, blue colour lower density.

Discussion Paper | Discussion Paper  
Inter-comparison of energy balance and hydrological models over a whole river catchment

R. Guzinski et al.

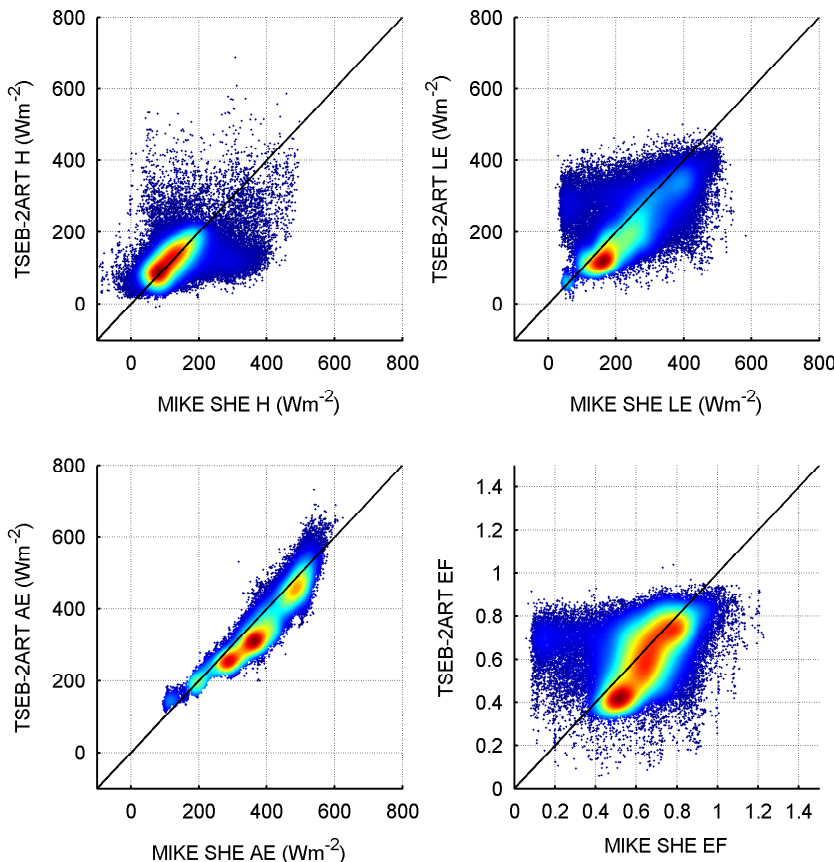


**Figure 3.** Density scatter plot of over 105 000 points comparing the sensible heat flux (top left), latent heat flux (top right), available energy (bottom left) and evaporative fraction (bottom right) modelled by MIKE SHE and TSEB-2ART. Red colour indicates higher density of points, blue colour lower density.

## Inter-comparison of energy balance and hydrological models over a whole river catchment

R. Guzinski et al.

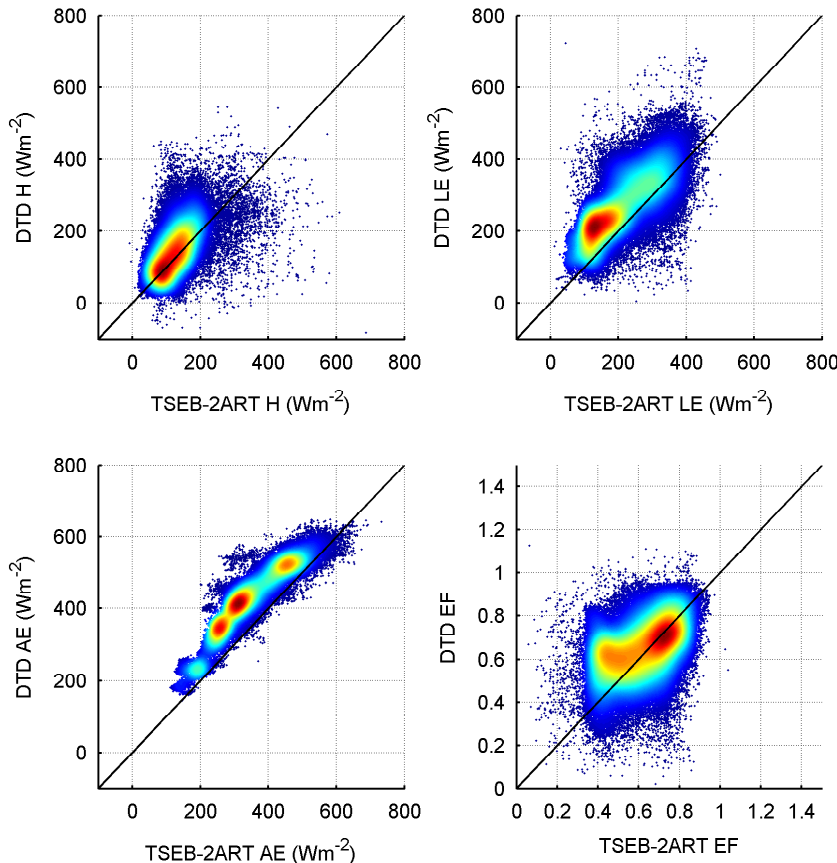


**Figure 4.** Density scatter plot of over 105 000 points comparing the sensible heat flux (top left), latent heat flux (top right), available energy (bottom left) and evaporative fraction (bottom right) modelled by TSEB-2ART and DTD. Red colour indicates higher density of points, blue colour lower density.

## Inter-comparison of energy balance and hydrological models over a whole river catchment

R. Guzinski et al.

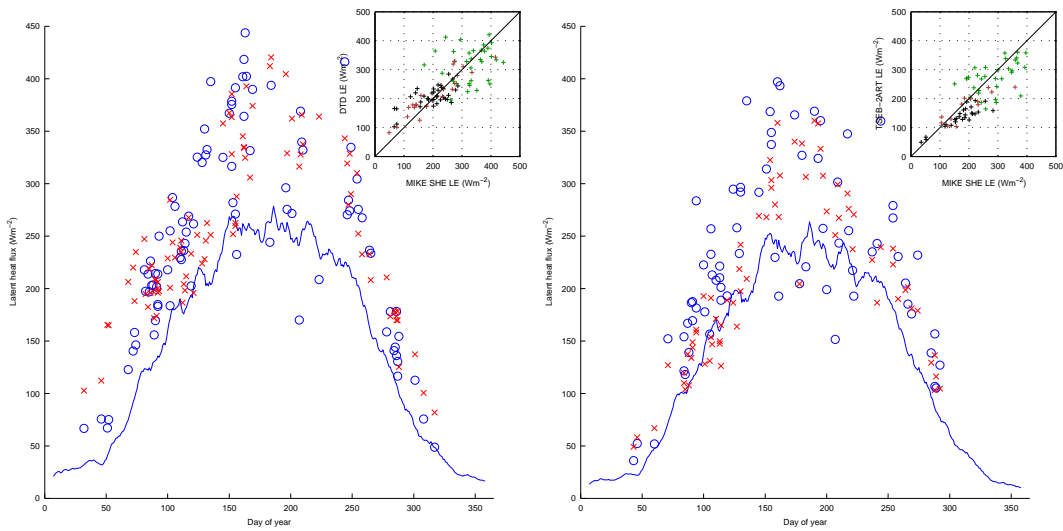


**Figure 5.** Average catchment-wide latent heat fluxes on the days when at least 80 % of non-water and non-urban pixels were modelled by either DTD (left) or TSEB-2ART (right). In the main graph the blue circles represent catchment fluxes modelled by MIKE SHE and the red crosses represent the catchment fluxes modelled by the remote sensing models on the same day-of-year (DOY) and at the same time of day. The figure contains dates from the seven years under investigation and the blue line shows the averaged, smoothed catchment fluxes for each DOY from those seven year modelled by MIKE SHE around the time of Aqua (left) or Envisat (right) overpass. The inset image contains a scatterplot of the MIKE SHE and remote sensing fluxes with black indicating fluxes from January to April, green from May to August and brown from September to December.

Title Page

## Abstract

## Introduction

## Conclusio

## References

## Tables

## Figures

1

1

Back

Close

Full Screen / Esc

[Printer-friendly Version](#)

## Inter-comparison of energy balance and hydrological models over a whole river catchment

R. Guzinski et al.

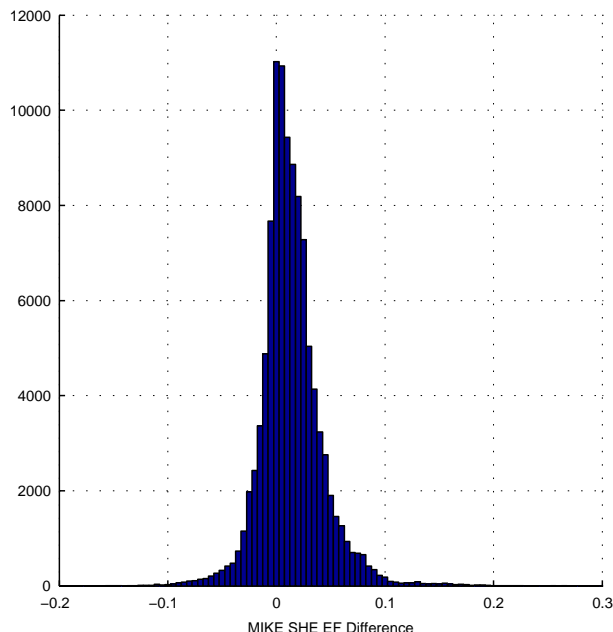


**Figure 6.** Histogram of the pixel-wise differences between Evaporative Fraction (EF) estimated by MIKE SHE at the time of Aqua overpass and Envisat overpass. The differences between the two sets were evaluated using the two-sample  $t$  test and are found to be statistically significant with a  $p$  value smaller than 0.001.

## Title Page

## Abstract

## Introduction

## Conclusio

## References

## Tables

## Figures

1

Ba

Close

Full Screen / Esc

Interactive Discussion

## Inter-comparison of energy balance and hydrological models over a whole river catchment

R. Guzinski et al.

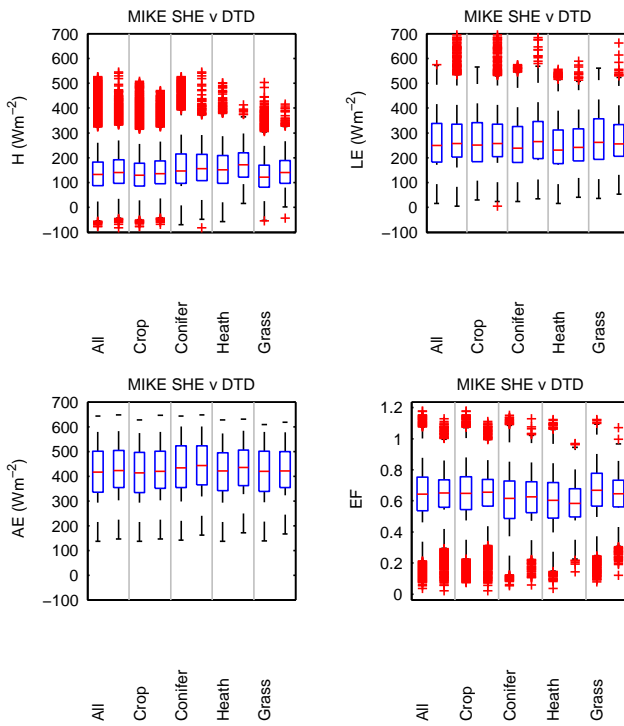


**Figure 7.** Box plots of sensible heat flux (top left), latent heat flux (top right), net radiation (bottom left) and evaporative fraction (bottom right) modelled by MIKE SHE (leftward box in each category) and DTD (rightward box in each category) and split by land cover class. The red horizontal line indicates the median value with the upper and lower box edges indicating the 75th and 25th percentiles respectively. The whiskers extend to the furthest point within 1.5 times the inter-box range above or below the box edges with points beyond that categorized as outliers and marked individually as a red crosses.

## Inter-comparison of energy balance and hydrological models over a whole river catchment

R. Guzinski et al.

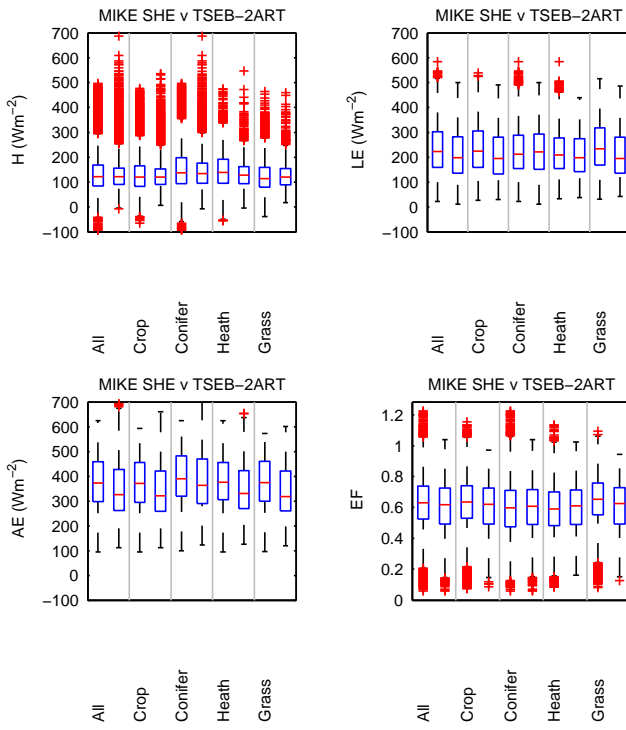


**Figure 8.** Box plots of sensible heat flux (top left), latent heat flux (top right), net radiation (bottom left) and evaporative fraction (bottom right) modelled by MIKE SHE (leftward box in each category) and TSEB-2ART (rightward box in each category) and split by land cover class. The red horizontal line indicates the median value with the upper and lower box edges indicating the 75th and 25th percentiles respectively. The whiskers extend to the furthest point within 1.5 times the inter-box range above or below the box edges with points beyond that categorized as outliers and marked individually as a red crosses.

## Inter-comparison of energy balance and hydrological models over a whole river catchment

R. Guzinski et al.

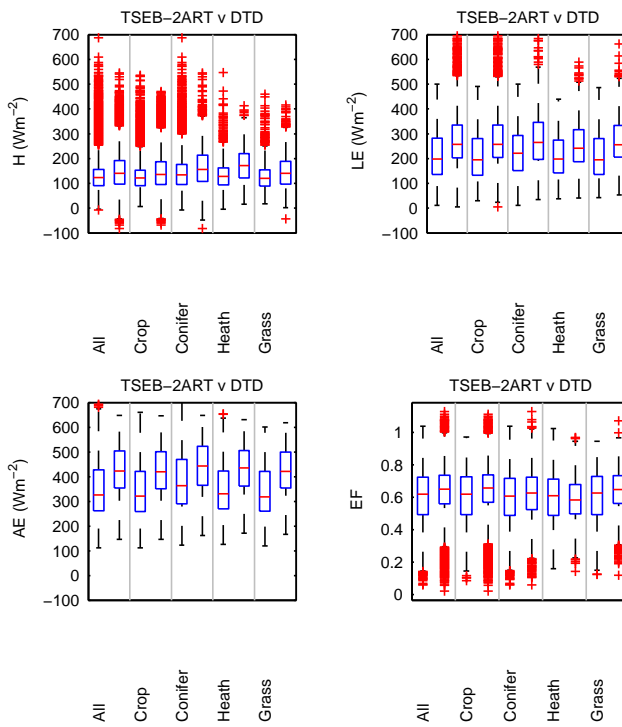


**Figure 9.** Box plots of sensible heat flux (top left), latent heat flux (top right), net radiation (bottom left) and evaporative fraction (bottom right) modelled by TSEB-2ART (leftward box in each category) and DTD (rightward box in each category) and split by land cover class. The red horizontal line indicates the median value with the upper and lower box edges indicating the 75th and 25th percentiles respectively. The whiskers extend to the furthest point within 1.5 times the inter-box range above or below the box edges with points beyond that categorized as outliers and marked individually as a red crosses.

**Inter-comparison of energy balance and hydrological models over a whole river catchment**

R. Guzinski et al.

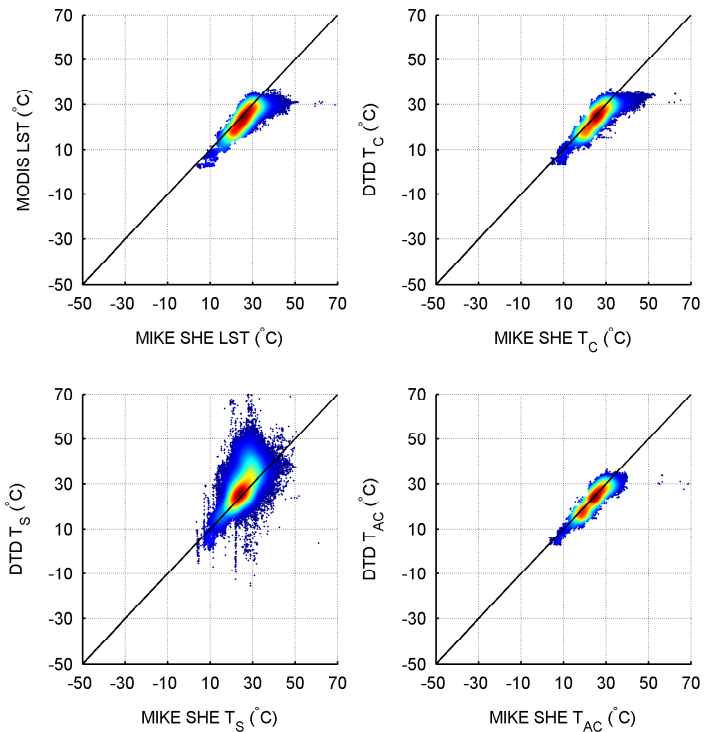


**Figure 10.** Density scatter plot of over 105 000 points comparing land surface temperature (top left), canopy temperature (top right), soil temperature (bottom left) and in-canopy air temperature (bottom right). Land surface temperature on the x-axis was modelled by MIKE SHE and on the y-axis came from day time observations from the MYD11A1 MODIS product. The other temperatures were modelled by both MIKE SHE and DTD. Red colour indicates higher density of points, blue colour lower density.

---

**Inter-comparison of energy balance and hydrological models over a whole river catchment**

R. Guzinski et al.

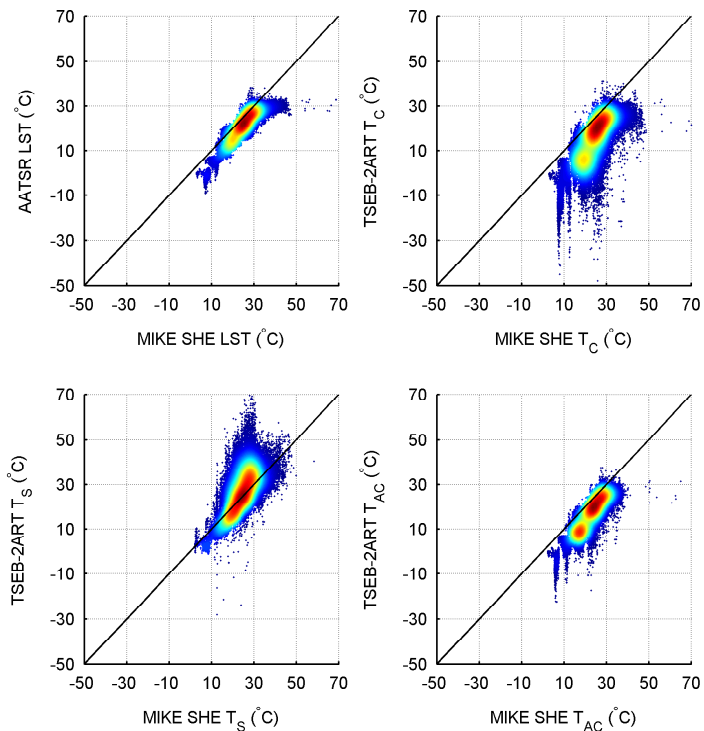


**Figure 11.** Density scatter plot of over 105 000 points comparing land surface temperature (top left), canopy temperature (top right), soil temperature (bottom left) and in-canopy air temperature (bottom right). Land surface temperature on the x-axis was modelled by MIKE SHE and on the y-axis came from nadir observations by AATSR sensor on the Envisat satellite. The other temperatures were modelled by both MIKE SHE and TSEB-2ART. Red colour indicates higher density of points, blue colour lower density.

**Inter-comparison of energy balance and hydrological models over a whole river catchment**

R. Guzinski et al.

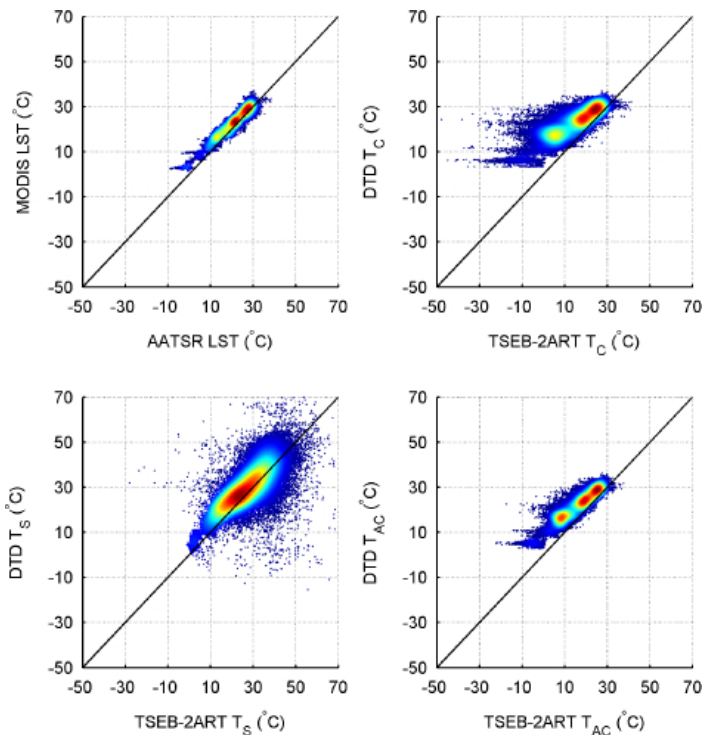


**Figure 12.** Density scatter plot of over 105 000 points comparing land surface temperature (top left), canopy temperature (top right), soil temperature (bottom left) and in-canopy air temperature (bottom right). Land surface temperature on the x-axis came from nadir observations by AATSR sensor on the Envisat satellite and on the y-axis came from day time observations from the MYD11A1 MODIS product. The other temperatures were modelled by both TSEB-2ART and DTD. Red colour indicates higher density of points, blue colour lower density.

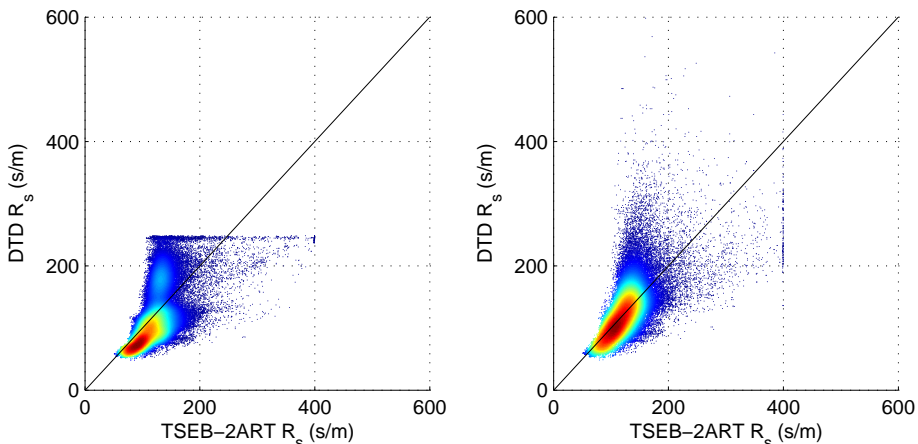


**Figure 13.** Density scatter plot of over 105 000 points comparing resistance of heat transfer from the soil surface ( $R_S$ ) modelled by the TSEB-2ART and DTD. In the left panel the original DTD formulation is used (Norman et al., 2000) and in the right panel the new formulation is used (Eq. 4). Red colour indicates higher density of points, blue colour lower density.

## Inter-comparison of energy balance and hydrological models over a whole river catchment

R. Guzinski et al.

## Title Page

## Abstract

## Introduction

## Conclusion

## References

## Tables

## Figures

14

1

1

1

Back

Close

Full Screen / Esc

Interactive Discussion